Macromolecular Chemistry and Physics
www.mcp-journal.de



# Precision Synthesis of Boron-Doped Graphene Nanoribbons: Recent Progress and Perspectives

*Jin-Jiang Zhang, Ji Ma,* and Xinliang Feng**

Special issue dedicated to Brigitte Voit on the occasion of her 60th birthday

**Structurally precision graphene nanoribbons (GNRs) have attracted great interest considering their prospective applications as organic carbon materials for nanoelectronics. The electronic properties of GNRs not only critically depend on the edge structure and width but also on the heteroatom type, doping position, and concentration. Motivated by the recent undisputable progress in the synthesis of stable boron-doped polycyclic aromatic hydrocarbons (B-PAHs), considerable efforts have been devoted to the precision synthesis of the corresponding boron-doped GNRs (B-GNRs) via bottom-up synthesis approach in recent years in view of the extraordinary ability of boron doping on modulating their physiochemical properties. In this review, an overview of the bottom-up organic synthesis of B-GNRs, including the precursor design and synthesis, structure characterization of the resulting B-GNRs, and investigation of their electronic properties is provided. Moreover, the future challenges and perspectives regarding the bottom-up synthesis of B-GNRs are also discussed. The authors hope that this review will further stimulate the synthesis and device integrations of B-GNRs with a combined effort from different disciplines.**

## 1. Introduction

Graphene nanoribbons (GNRs), structurally confined quasi-1D graphene strips, have displayed unique optical, electronic and magnetic properties,[1–4] which are regarded as promising candidates for various electronic applications, such as field-effect transistors (FETs), spintronic devices and quantum computing.[5–7] Whereas the prevailing "top-down" approaches, such as hydrothermal or lithographic "cutting" of graphene, cannot control the topology structures or size distributions of GNRs, and "bottom-up" chemical synthesis has been developed to provide GNRs with structural precision. Bottom-up synthetic method toward GNRs usually bases on two main pathways, namely: 1) using synthetic organic and polymer chemistry techniques;[8] and 2) on-surface assisted method with modern surface science techniques.[9] In the last decade, both in-solution and on-surface synthesis have significantly advanced in a highly complementary manner for the development of atomically precise GNRs, and enabling a variety of GNRs with different topologies so that their structure–property relationships can be insightfully studied. It has been shown that the electronic properties of GNRs critically depend on their edge structures and widths. According to the edge topology, GNRs can be classified into different types, such as armchair-edged GNRs (AGNRs), zigzag-edged GNRs (ZGNRs), cove-edged GNRs (CGNRs) and chiral GNRs with mixed edges (**Figure 1**).[10] Among them, both the AGNRs and CGNRs, particularly for those width is narrower than 10 nm, exhibit semiconducting behavior with a direct band gap,[11,12] whereas the ZGNRs possess half-metallic properties with zero bandgap (based on the tight-binding theory), showing strongly localized charge density of the edge state at the zigzag sites.[13–15] On the other hand, the edge configuration of chiral GNRs bearing the armchair and zigzag edges are characterized by a chiral vector (n, m) which connects crystallographically equivalent sites along the edge, and their physiochemical properties, such as electronic band structures and magnetic properties, are highly dependent on the chiral vector.[16]

Besides the edge structure and width control, the introduction of heteroatoms into GNRs also represents a feasible strategy to tune their optical, electronic and magnetic properties.[17,18] In this regard, both the heteroatom type, doping position, and doping concentration exhibit significant influence on the electronic band structure and charge carrier concentration of heteroatom-doped GNRs. In addition to the primary dopant elements (e.g., nitrogen, oxygen, sulfur) in graphene carbon framework, boron

J.-J. Zhang, J. Ma, X. Feng
Center for Advancing Electronics Dresden (cfaed) & Faculty of Chemistry and Food Chemistry
Technische Universität Dresden
01062 Dresden, Germany
E-mail: ji.ma@tu-dresden.de; xinliang.feng@tu-dresden.de
X. Feng
Department of Synthetic Materials and Functional Devices
Max Planck Institute of Microstructure Physics
06120 Halle, Germany

The ORCID identification number(s) for the author(s) of this article can be found under https://doi.org/10.1002/macp.202200232



**DOI: 10.1002/macp.202200232**

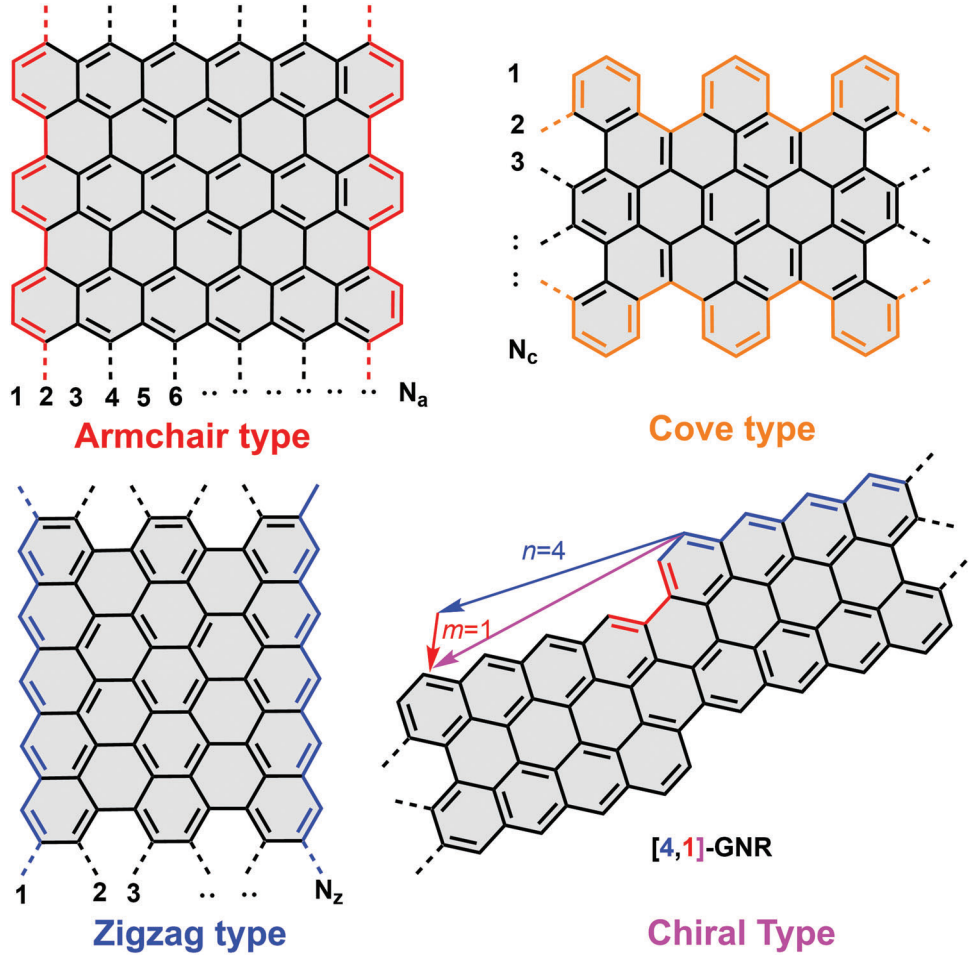


**Figure 1.** Structures of armchair type, zigzag type, cove type, and chiral type GNRs. The width of the AGNRs, ZGNRs and CGNRs are depicted as the numbers "$N_a$", "$N_z$" and "$N_c$", respectively. The edge geometry of chiral GNRs is characterized by the translation vector [n, m].

(B) is a unique dopant in view of its electron deficiency and Lewis acidity, which may offer a wide variety of functionality in GNRs. To take the small size B-doped polycyclic aromatic hydrocarbons (B-PAHs) as examples, the boron doping endows the resultant heteroaromatic system with a $\pi$-electron-acceptor site due to the existence of vacant $p_z$ orbital of boron, which can be used to stabilize some reactive species, such as radical containing compounds, through electron delocalization (**Figure 2**).[19,20] On the other hand, B-PAHs could also simultaneously act as $\sigma$-donors because boron has lower Pauling electronegativity (EN(B) = 2.0) compared with carbon (EN(C) = 2.6).[21] In addition, B-PAHs are capable of forming Lewis acid–base complex with various Lewis base, which could display unique optical properties, such as dual fluorescence.[22] Furthermore, B-PAHs generally have energetically low-lying LUMO and narrow HOMO–LUMO gaps, which are highly desirable for n-type or ambipolar semiconductor materials.[23] Most importantly, B-PAHs usually show magnificent fluorescence with high photoluminescence quantum yield, thus making them promising emitter materials for OLED applications.[24–26]

Nevertheless, the $p_z$ orbital of boron also brings the instability issue in the heteroatom-doped PAH system, because boron center can easily be attacked by nucleophilic species due to its high electrophilic feature. Hence, addressing the instability issue of B-PAHs becomes particularly important, not only for revealing the structure–property relationship of B-PAHs but also for advancing the development of B-doped GNR (B-GNR) chemistry. To achieve this, three strategies have been generally explored so far to address the stability problems of B-PAHs, including electronic effect,[23,27–29] steric effect[30–33] and chelating effect[34–39] (**Figure 3**). These established methodologies pave the way for boron doping of GNRs by using the predesigned stable organoboron precursors. Although considerable progress has been made in the synthesis of bench-stable B-PAHs, the bottom-up chemical synthesis of their related B-GNRs is still scarce due to the limited precursor molecules containing boron atoms and the lack of suitable synthetic strategies. In this review article, we provide an overview of the synthetic efforts toward the structurally defined B-GNRs via bottom-up on-surface or in-solution synthetic approach, as well as the related boron-containing precursor design. Moreover, the electronic properties of the resultant B-GNRs are also presented. Finally, we also provide our views on the challenges and perspectives regarding the precision synthesis of B-GNRs.

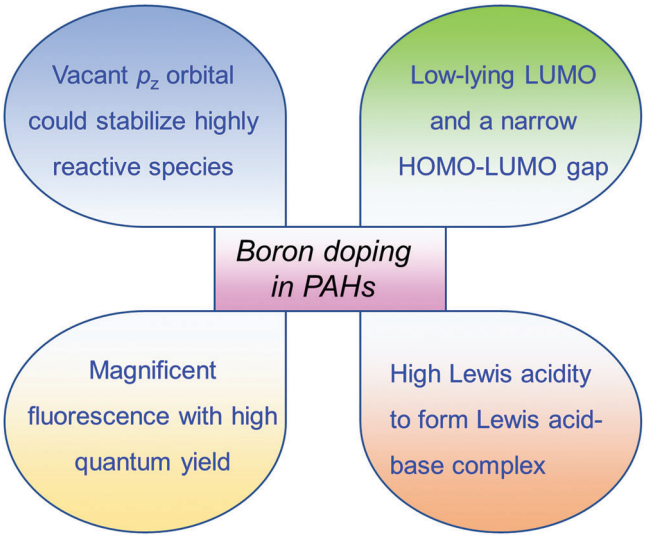


**Figure 2.** The wide scope of functionalities in B-doped PAHs.

## 2. On-Surface Synthesis of B-GNRs

For on-surface assisted method toward B-GNRs, it usually involves three steps: i) sublimation of dihalogenated boron-doped monomers onto a metal surface under ultrahigh vacuum conditions (UHV); ii) surface-assisted formation of diradical intermediates and homocoupling polymerization; and iii) surface-assisted cyclodehydrogenation by annealing at a higher temperature. The most attractive feature of the on-surface assisted method is that the resulting GNRs can be visualized in situ by high-resolution scanning tunneling microscopy (STM) under UHV conditions, unambiguously proving their atomically precise structures.

In 2015, Fischer group and Kawai group independently reported boron-doped 7-AGNR (B-7-AGNR) **5** via on-surface synthesis.[40,41] As shown in **Figure 4**a, the preparation of B-7-AGNR **5** was achieved through two major steps starting from boron-containing precursor **3**, which was obtained through the treatment of selectively mono-lithiated 9,10-dibromoanthracene (**2**) with 5,10-dibromo-5,10-dihydroboranthrene (**1**). First, precursor **3** was deposited on an Au(111) surface under UHV condition and was subsequently annealed at 180 °C to afford linear polymer **4** via surface-catalyzed dehalogenative polymerization. Subsequently, the elevation of annealing temperature to 400 °C triggered the surface-assisted cyclodehydrogenation to produce B-7-AGNR **5**. The chemical structure of **5** was directly resolved by STM and high-resolution non-contact atomic force microscopy (nc-AFM) equipped with a CO functionalized tip, which indicated that the boron atoms were indeed located at the center of the GNRs, corresponding to 4.8 atom percentage (Figure 4b–d). To elucidate its electronic structure, the d$I$/d$V$ studies were conducted for **5** and the bandgap was estimated to be 2.4 eV (Figure 4e), which was comparable to the non-doped 7-AGNR (2.3 eV) on Au(111). This result showed that B-doping in **5** did not influence the overall electronic structure of the pristine 7-AGNR. Due to the Lewis acidity of boron centers, **5** was found to efficiently adsorb NO, which was demonstrated by STM topography as well as simulated STM image, indicating that B-GNRs could be used as gas sensor materials. In addition, it was also observed that the armchair edges of **5** could fuse at high temperature (500 °C), leading to the formation of B-GNRs with wider widths of $N = 14$ and $N = 21$ (Figure 4f). More detailed studies on the electronic properties of B-GNR **5** were demonstrated by Garcia-Lekue, Corso, Pascual et al.[42,43] They revealed that the electronic band gap of B-GNR **5** could be finely tuned by varying the distance between two boron atoms. Besides, rotation of the boron-containing moiety with respect to the ribbon axis can change the symmetry of the carbon bands that they mix with, which should have an effect on the frontier transport bands.

In 2020, the evolution of a magnetic ground state was achieved by inserting a pair of B atoms in 7-AGNRs by Pascual and coworkers (**Figure 5**a).[44] The 10,10′-dibromo-9,9′-bianthryl precursor **6** along with a small portion of B-doped molecule **3** were evaporated and allowed for surface-assisted polymerization and cyclodehydrogenation. The structure of the resultant B-7-AGNR **7** was confirmed by the STM study (Figure 5b). The doping of a pair of B atoms broke the conjugation of their topological bands and consequently, two spin-polarized boundary states around them were generated. The spin state was detected in electrical transport measurements through **7** suspended between a tip and sample. Most recently, by using first-principles calculations, Zhang et al. demonstrated that the magnetism in B-7-AGNR **7** is contributed by $\pi$-electrons, originating from the imbalance of electrons in two spin channels in response to boron dopants (Figure 5c).[45]

In 2018, Kawai, Hatakeyama, Foster et al. reported the synthesis and characterization of a defined GNR embedded with B/N co-doping starting from functionalized dibenzoazaborine monomer **12** (**Figure 6**a).[46] The 10-bromo-5-(10-chloroanthracen-9-yl)-5,10-dihydrodibenzo[*b*,*e*][1,4] azaborinine (**9**) was obtained through an intramolecular tandem electrophilic borylation from compound **8**. Then, treatment of **9**

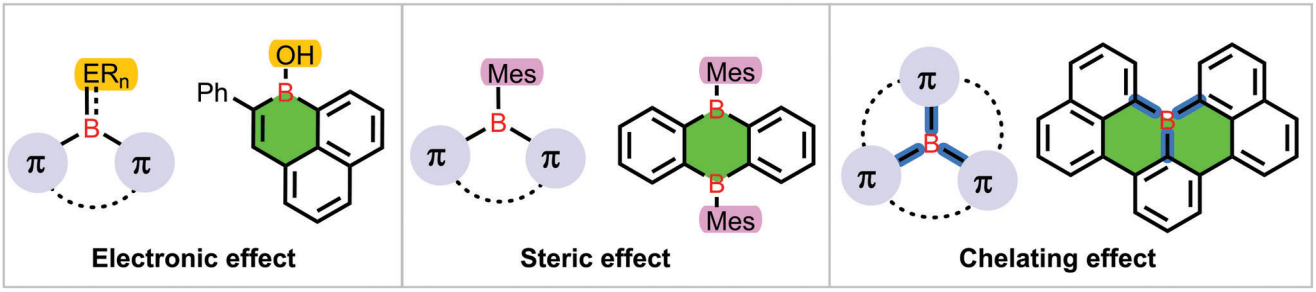


**Figure 3.** Three strategies for making bench-stable B-PAHs and representative examples.

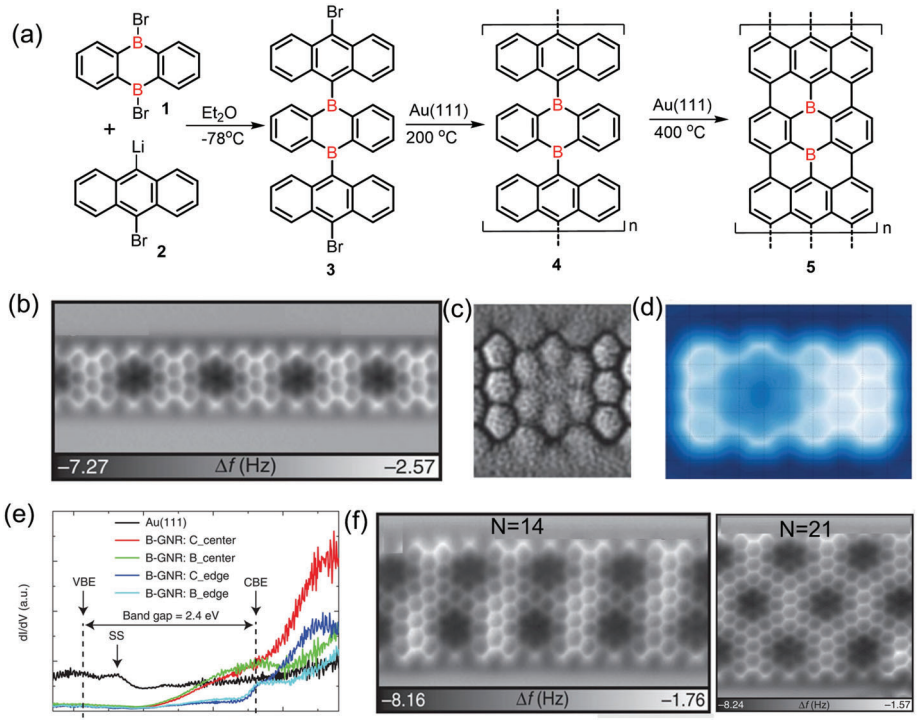


**Figure 4.** a) Schematic illustration of the on-surface synthesis of B-7-AGNR (**5**); b) the nc-AFM image and c) the Laplace filtered image of **5** taken using a CO-functionalized tip; d) the simulated AFM image of **5**; e) d*I*/d*V* curve on B-7-AGNR **5**; f) Δ*f* maps of fused *N* = 14 B-AGNR and *N* = 21 B-AGNR. (b–f) reproduced with permission.[40] Copyright 2015, Springer Nature.

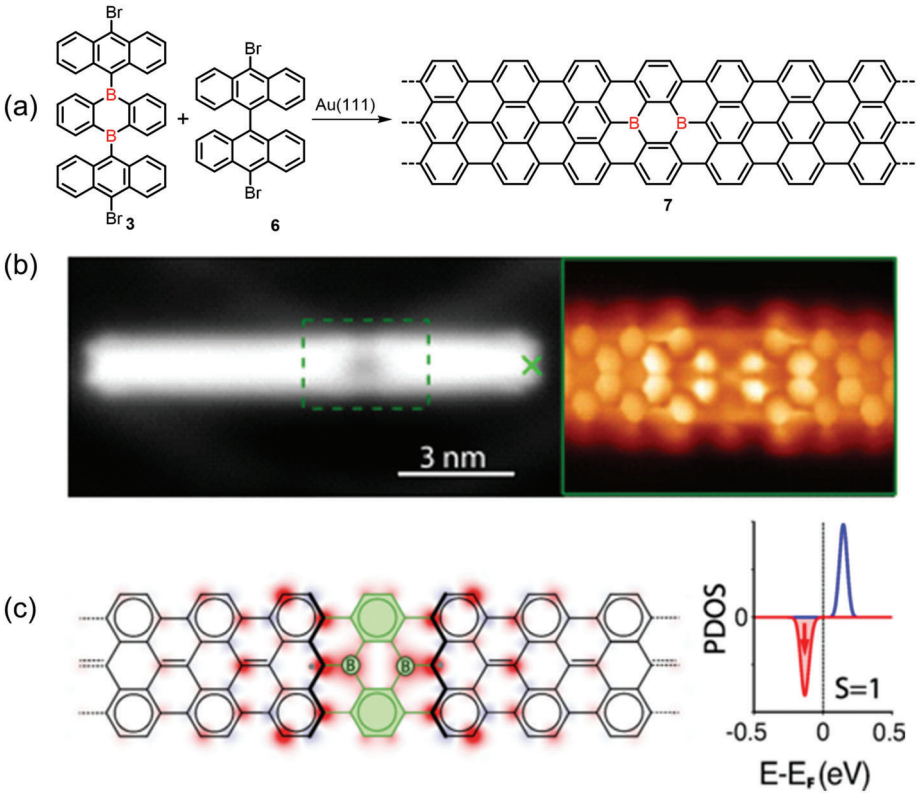


**Figure 5.** a) Schematic drawing of the synthesis of B-7-AGNR (**7**) on Au(111)surface; b) STM constant current topography image and constant height current scan of **7**; c) simulated structure of the 2B-7AGNR by DFT calculations (left) and spin-resolved projected density of states (PDOS) over carbon atoms around two boron atoms (right). (b,c) reproduced with permission.[44] Copyright 2020, American Physical Society.

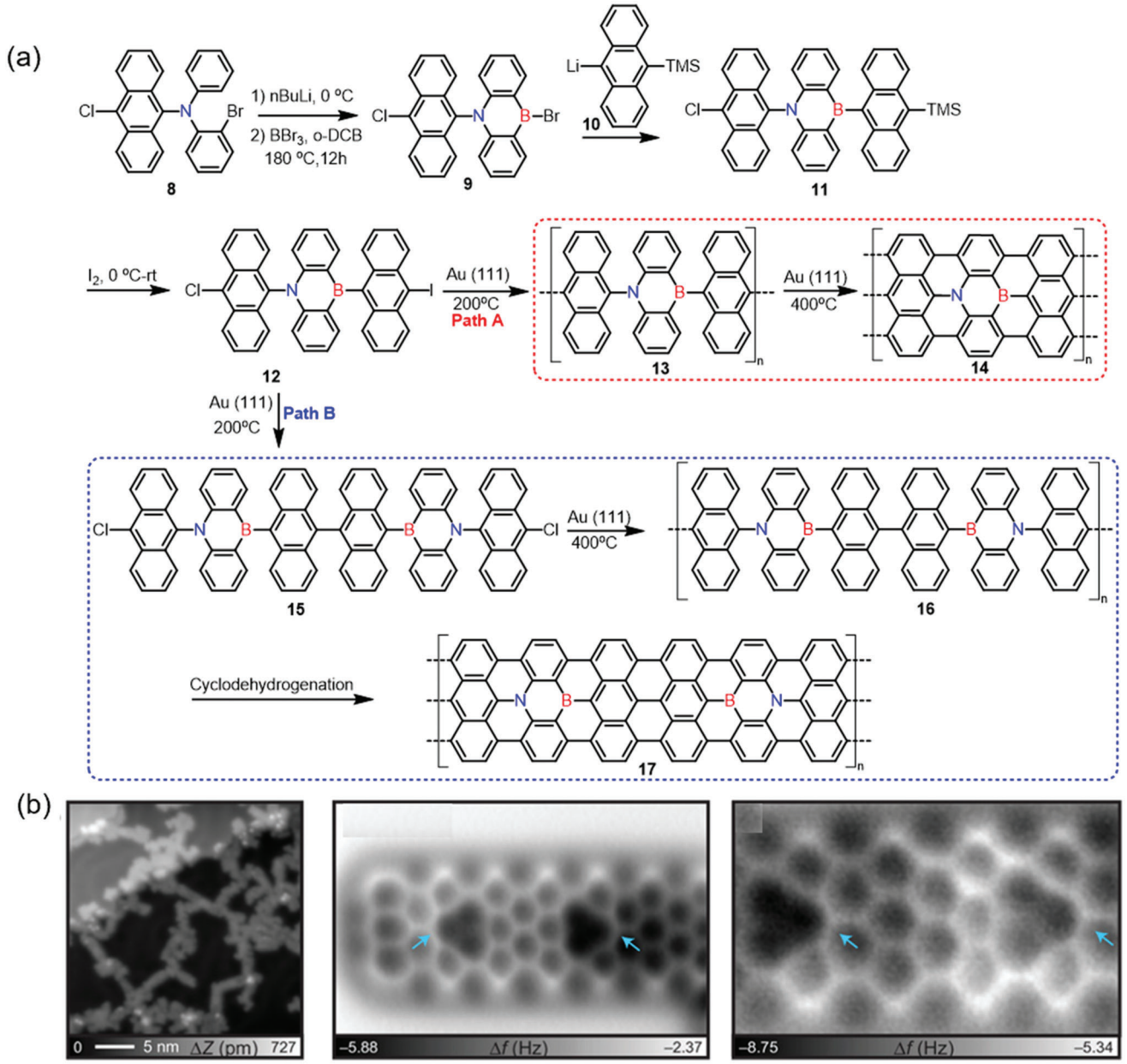


**Figure 6.** a) The synthetic route toward BN-7-AGNRs **14** and **17** via on-surface assisted approach; b) STM topography of the synthesized BN-7-AGNRs (left) and corresponding AFM images (middle is **17**, right is **14**). (b) reproduced with permission[46] Copyright 2018, American Association for the Advancement of Science.

with (10-(trimethylsilyl)-anthracene-9-yl)lithium (**10**), followed by replacing trimethylsilyl group with iodine, afforded **12** in a yield of 8.6%. For the on-surface synthesis of B/N-GNR, precursor **12** was first annealed on Au(111) surface at 200 °C to produce polymer **13** and dimer **15** through Cl–I coupling (Path A) and I–I coupling (Path B) reactions, respectively. Upon elevation of the annealing temperature to 400 °C, both polymer **13** and dimer **15** were converted into atomically precise BN-7-AGNR **14** and **17**, respectively. AFM observation with a CO-functionalized tip directly resolves the elemental difference in resultant BN-GNR, which can be correlated to the van der Waals radii, as well as the modulated local electron density caused by the substitution (Figure 6b). Besides, STM and density functional theory (DFT) calculations were also conducted to verify the structure and electronic properties of the resultant BN-7-AGNRs.

All the boron centers in the above B-doped AGNRs are embedded in the ribbon backbone and the tricoordinate boron formed covalent bonds with carbon atoms. In addition, other types of B-GNRs were also synthesized on the surface, in which the boron atom is located on the edges and the boron is attached to other heteroatoms, such as oxygen or nitrogen. Compared with AGNRs with boron dopants inside the ribbon backbone, the introduction of boron atoms on the edges has been shown

 

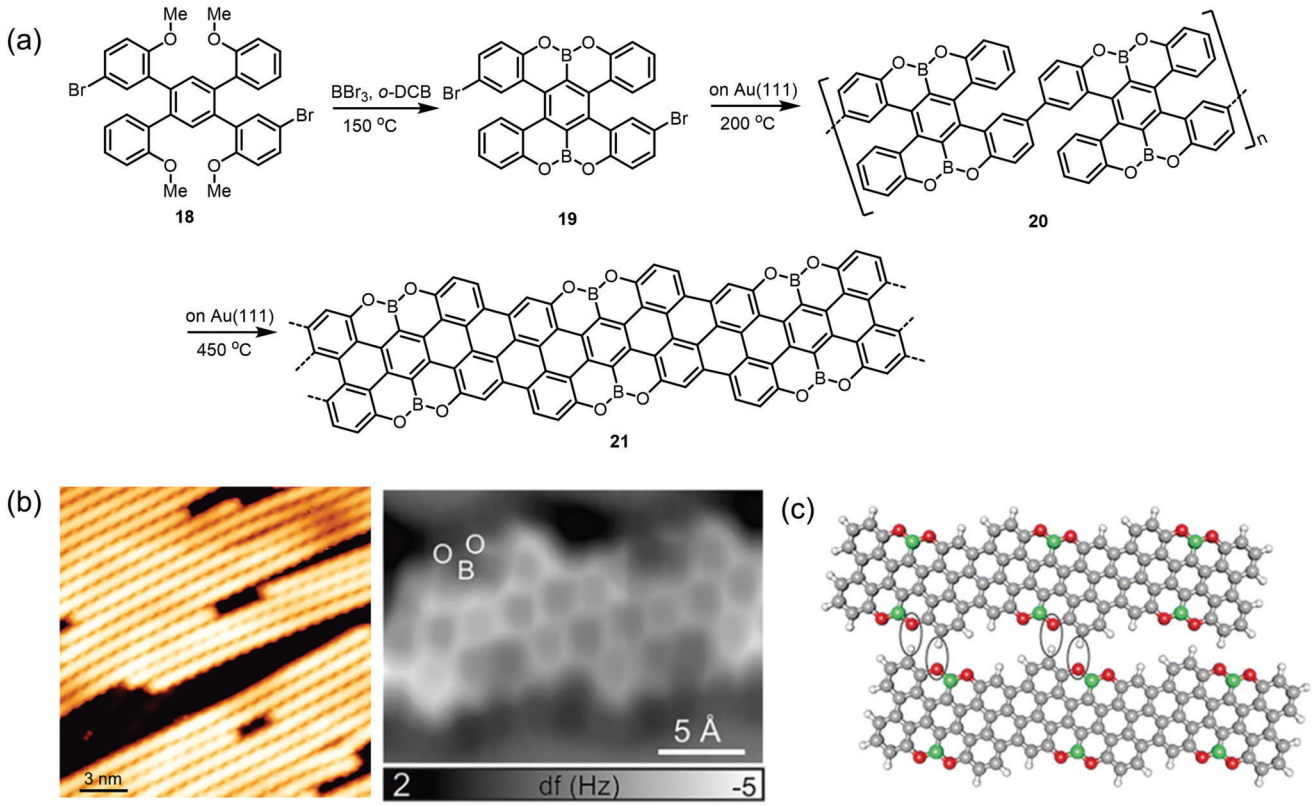


**Figure 7.** a) The synthetic route toward OBO-doped chiral (4,1)-GNR **21**; b) STM overview of **21** (left) and constant-height frequency-shift nc-AFM image of the ribbon segment (right); c) DFT models of inter-ribbon interactions for homochiral OBO-doped (4,1)-GNRs. (b,c) reproduced with permission.[47] Copyright 2018, American Chemical Society.

to impart unique properties on GNRs, such as self-assembly behavior.

In 2018, Müllen, Fasel, and our group reported the on-surface synthesis of the first chiral (4,1)-GNR **21** with OBO co-dopants from the rationally designed precursor 6,16-dibromo-9,10,19,20-tetraoxa-9a,19a-diboratetrabenzo[*a,f,j,o*]perylene (**19**) (**Figure 7**a).[47] Precursor **19** was synthesized in decent yield through a tandem demethylation–borylation reaction from 1,4-bis(5′-bromo-2′-methoxyphenyl)-2,5-bis(2′-methoxyphenyl)-benzene (**18**). To fabricate the OBO-doped chiral (4,1)-GNR **21**, monomer **19** was first sublimed onto an Au(111) substrate held at room temperature under UHV conditions, followed by annealing the substrate at 200 °C to induce polymerization and further annealing the polymer at 450 °C to initiate cyclodehydrogenation, fully planarized OBO-doped chiral (4,1)-GNR **21** with an average length of 61 nm was finally obtained. The structure of **21** was characterized by STM and nc-AFM (Figure 7b) as well as Raman spectroscopy. DFT calculations combined with STS studies were conducted to unravel its band structure and the bandgap is identified to be 3.33 eV, which is in good agreement with the calculated bandgap (2.96 eV). Besides, DFT calculations reveal that the OBO-doped (4,1)-GNR **21** exhibits a larger bandgap (1.50 eV) in vacuum compared with the pristine all-carbon (4,1)-GNR (0.50 eV) due to the weak conjugation of the $p_z$ orbitals of the OBO segments with the carbon backbone of GNR. Moreover, the interaction energy of the structurally equivalent pristine (4,1)-GNR was calculated to be −0.10 eV/unit cell, indicating that the OBO units on the edges endow the GNRs with stronger inter-ribbon interactions (Figure 7c). Recently, the large-scale synthesis of OBO-doped (4,1)-GNR from precursor **19** was demonstrated by the chemical vapor deposition (CVD) method.[48] Noteworthily, stable and large-area OBO-doped (4,1)-GNR films could be obtained by a wet chemistry transfer process and the optical bandgap of the obtained GNR film is ≈1.9 eV.

Although OBO-doping could stabilize the zigzag edges of the resultant GNR and fine-tune its band structure, it significantly diminishes the electronic conjugation of the GNR, and thus does not contribute to improving its charge transport properties. In contrast, substituting C=C–C unit on the zigzag edge with a nitrogen–boron–nitrogen (NBN) motif not only provides access to stable ZGNRs but also renders the formation of the radical cation on the NBN unit through selective oxidation, which is the isoelectronic structure of its pristine carbon framework with an open-shell character.

In 2020, our group reported the first bottom-up synthesis of NBN-doped Z-GNRs through surface-assisted synthesis based on the U-shaped molecular oligoarylene precursors with an NBN unit preinstalled at the zigzag edge.[49] First, 4,13-bis(4-iodophenyl)-2-phenyl-8*H*,9*H*-8,9-diaza-8a-borabenzo-[*f,g*]tetracene (**23a**) was synthesized through multistep organic synthesis, in which the NBN motif was introduced to the zigzag periphery by $NH_2$-directed electrophilic borylation. Then, monomer **23a** was deposited onto the gold substrate

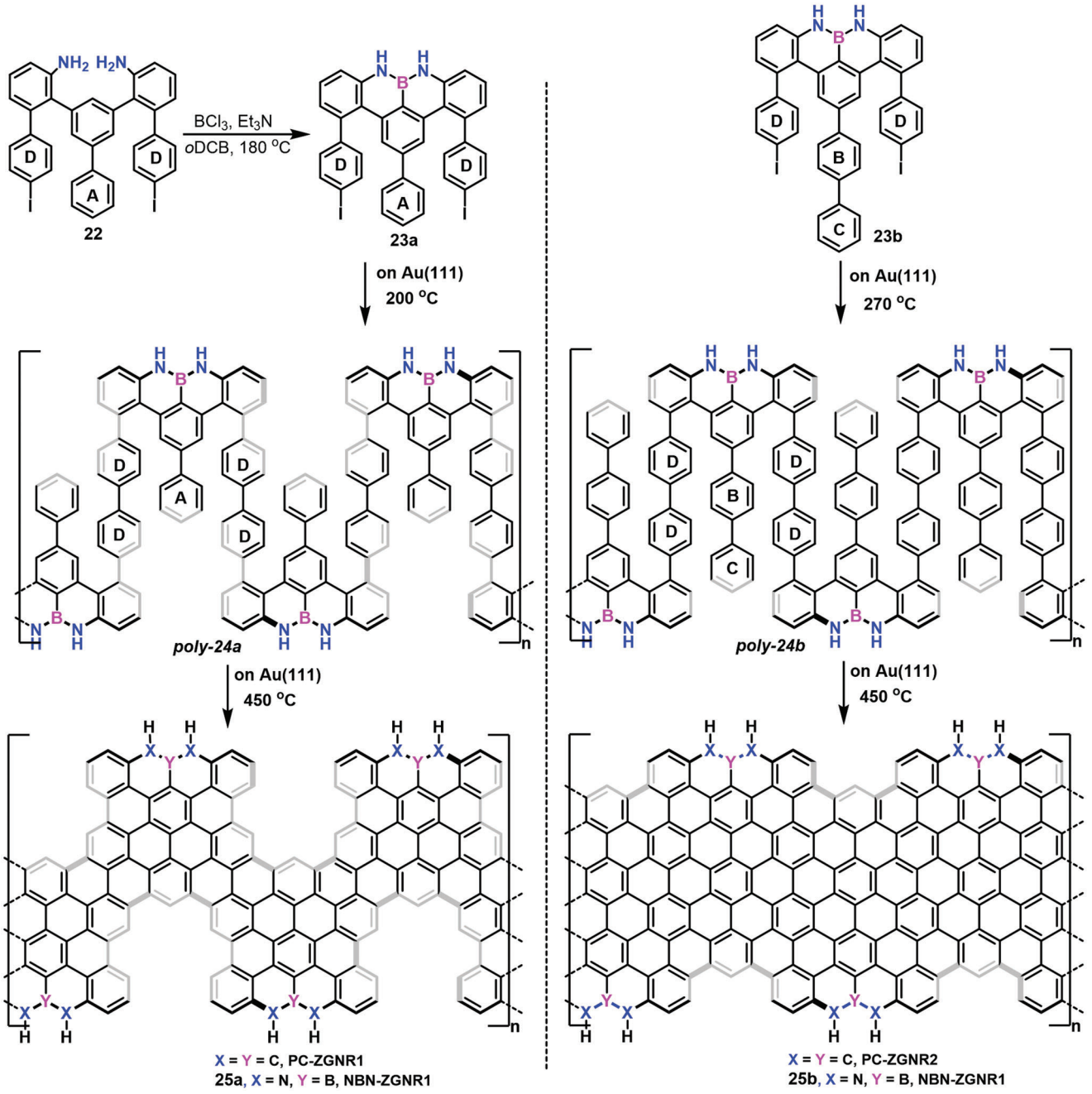


**Figure 8.** Synthetic strategy for NBN-doped ZGNR1 **25a** and ZGNR2 **25b**.

and the swallow-shaped polymer **poly-24a** was synthesized by annealing at 200 °C (**Figure 8**, left). Subsequently, the targeted NBN-ZGNR1 (**25a**) could be obtained through intramolecular cyclodehydrogenation of **poly-24a** at 450 °C. Similarly, monomer **23b** containing one additional phenyl ring was further developed to synthesize NBN-ZGNR2 (**25b**) (Figure 8, right), in which the zigzag edge proportion (57%) was larger than that of NBN-ZGNR1 (37%). However, the length of NBN-ZGNR2 is shorter than that of NBN-ZGNR1 due to the increased steric hindrance between the central benzene rings (ring B and C) with the side rings (ring D) in the polymer **poly-24b**.

The zigzag edge topologies of both NBN-ZGNRs were evidently unveiled through STM and nc-AFM measurements (**Figure 9**a–c). Comparing the electronic structures of pristine carbon-based ZGNRs (**PC-ZGNRs**) without NBN units (**PC-ZGNR1**: 0.52 eV, Figure 9e; **PC-ZGNR2**: 0.27 eV, Figure 9g), the energy bandgaps of NBN-ZGNR1 (1.50 eV, Figure 9d) and NBN-ZGNR2 (0.90 eV, Figure 9f) are much higher, indicating that NBN doping plays a significant role in tailoring the electronic structures of GNRs. Moreover, theoretical calculations predict that the band structures of NBN-ZGNRs can be further tailored to be gapless or metallic through the

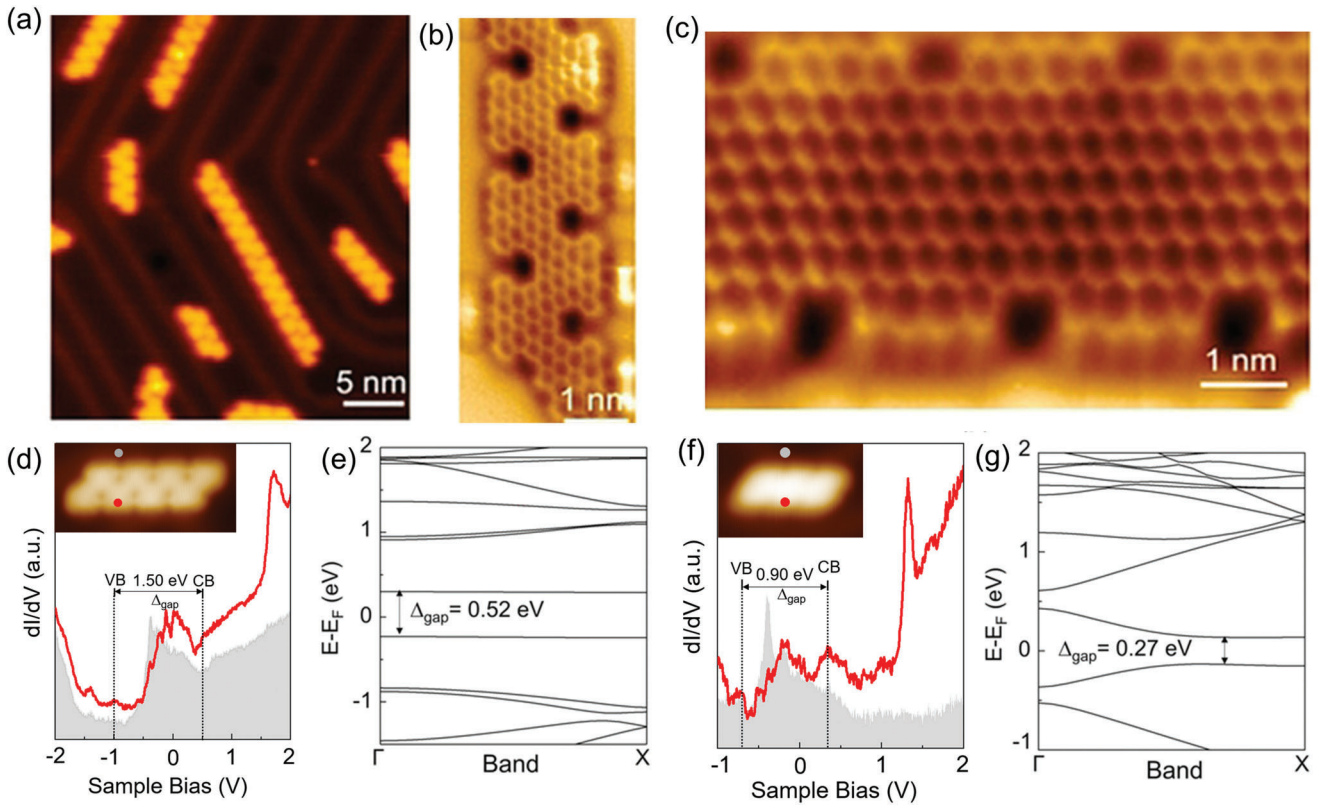


**Figure 9.** a) STM image and b) nc-AFM image of ZGNR1 (**25a**); c) nc-AFM image of ZGNR2 (**25b**); (d) and (f) STS and calculated band structures of **25a** and **25b**; (e) and (g) DFT-calculated band structures of pristine carbon-based **PC-ZGNR1** and **PC-ZGNR1**. (a,g) reproduced with permission.[49] Copyright 2020, Wiley-VCH GmbH.

selective oxidation of the NBN units into the formation of radical cations.

## 3. In-Solution Synthesis B-GNRs

Besides the on-surface synthesis, solution synthesis also presents an alternative strategy to provide well-defined GNRs. For solution synthesis, it usually consists of two steps: i) the polymerization of small molecular precursors for making polyarylenes (polymer precursors); and ii) the subsequent graphitization, so-called cyclodehydrogenation. Solution-synthesis approaches show significant advantages for the large-scale preparation of liquid-phase-dispersible GNRs with controlled structures. To date, almost all the reported B-GNRs have been achieved via the surface-assisted synthesis which requires the pre-installation of boron centers in the molecular precursors. In contrast, due to the high flexibility and easy-to-handle features of in-solution synthesis, GNRs obtained through this approach allow for post-functionalization of resultant GNRs by introducing the boron element in the final stage.

In 2018, Dong and co-workers realized the solution synthesis of B-6-AGNRs (**32**) by post-functionalization of 6-AGNRs (**31**) containing thiazole units (**Figure 10**). At first, model compound **27**, which can be regarded as the short segments of B-6-AGNRs (**32**), was synthesized to demonstrate the feasibility of the borylation reaction (Figure 10a). C–H borylation of **26** was successful upon simple treatment of it with $BCl_3$; subsequently, addition of $ZnPh_2$ afforded **27** in 64%, which was fully characterized by $^1H/^{13}C$ NMR, X-ray crystallography and mass spectroscopy. The synthesis of **32** is illustrated in Figure 10b. At first, the Suzuki–Miyaura polymerization of monomers **28** and **29** formed linearly polymer precursor **30**.[50] The following cyclodehydrogenation reaction of **30** furnished GNR **31** in excellent yield. The optical band gap of thiadiazole-fused GNR **31** was 1.03 eV, whose value is lower than that of the pristine 6-AGNR. Borylation of GNR **31** was conducted with a similar protocol on the synthesis of model compound **27**, affording the stable B-GNR **32**. Inductively coupled plasma-mass-spectrometry (ICP-MS) showed that the boron/sulfur (B:S) ratio in **32** was 0.38:1.00, indicating that the borylation efficacy was ≈38%. Besides, Raman spectrum of **32** exhibited higher $I_D/I_G$ than **31**, supporting the presence of enlarged edge regions caused by the formation of boracycles. Unsurprisingly, B-GNR **32** possessed a slightly narrower optical band gap of 0.95 eV compared with that of parent GNR **31**. This result reveals that post-functionalization is a straightforward strategy for tailoring the band gap of GNRs.

## 4. Summary and Outlook

In summary, this review provides an overview of the recent development of precision synthesis of B-GNRs either by on-surface assisted method or solution-mediated strategy. Although significant progress has been achieved, the efficient and diverse synthesis of B-GNRs is still in its infancy. Many challenges and

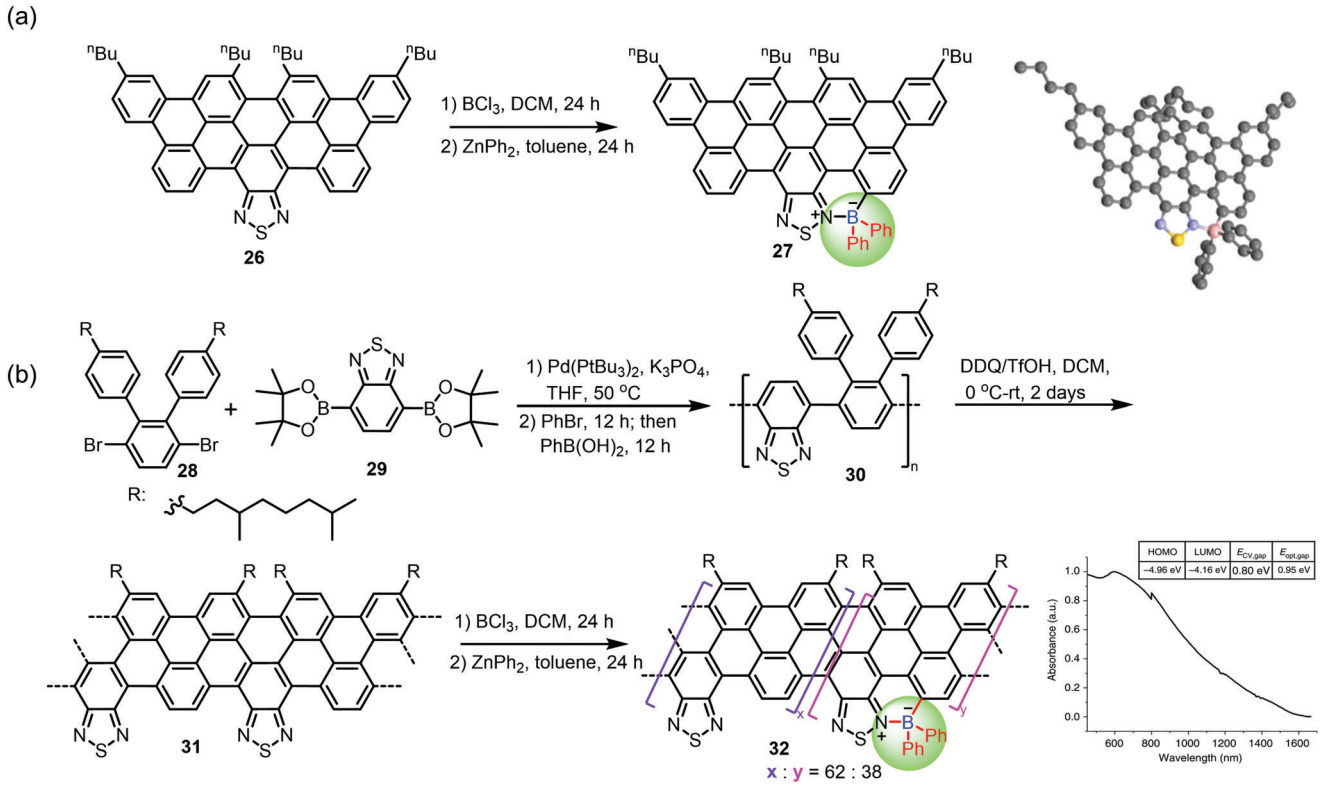


**Figure 10.** a) The borylation reaction of **26** afforded model compound **27**; b) the synthetic route toward GNR **31** and the post-functionalization of **31** through unsymmetrical heterocyclic edges as well as the UV–vis–NIR spectrum of **32** in THF suspension. (a,b) reproduced with permission.[50] Copyright 2018, Springer Nature.

opportunities remain for the synthetic exploration of this elusive type of GNRs, some of which are listed here:

i. Both the surface-assisted and in-solution strategies require pre-designed boron-containing precursor, however, the current studies have not paid enough emphasis on the novel precursor design for B-GNRs. Therefore, only a few B-doped precursors, such as 3 and 8 with diboraanthracene or dibenzoazaborine subunits, have been successfully employed for the synthesis of B-doped AGNRs. So far, only B-7-AGNRs could be achieved by surface-assisted approach, which is not beneficial to systematically investigate the influence of boron doping on their physicochemical properties. Although OBO/NBN doping at the zigzag edges of GNRs can be considered as a feasible strategy to stabilize the highly reactive zigzag edges and to enrich the B-GNR family, B-GNRs with cove and full zigzag edge topologies are still missing. In this regard, not only the exploration of synthetic methodologies toward stable B-PAHs, but also the design of B-PAHs could be potentially employed as precursors for synthesizing B-GNRs are the key factors for the further development of this field.
ii. On-surface synthesis allows for in situ characterization and direct measurement of the electronic properties of the resultant B-GNRs. Nevertheless, the mass production, purification, and isolation of B-GNRs are fundamentally difficult. Therefore, the large-scale synthesis and length control of GNRs by on-surface synthesis approach will be anticipated.[48]
iii. Although the surface-assisted synthesis of several types of B-GNRs has been demonstrated, in-solution synthesis of B-GNRs still lags behind. There is still no report on the in-solution synthesis of B-GNRs from the corresponding precursor with boron atoms, possibly due to the difficulty of the cyclodehydrogenation reaction where an electron-deficient boron-containing precursor is concerned. The introduction of strong electron donor groups into those precursors can be a feasible strategy to achieve the synthesis of B-GNRs in solution. On the other hand, the matrix assisted direct (MAD) transfer technique may provide an alternative pathway that requires the synthesis of B-doped polymer precursor featuring narrow and well-defined length distributions by solution-based polymerization methods, and then transferring the polymer precursor onto metal substrates for the cyclodehydrogenation process.[51]

We hope that, with this comparative assessment, this review will inspire new ideas in the design and synthesis of B-GNRs with novel structural topologies and functionalities, which will be strongly needed for the future development and integration of this type of unique GNRs in nanoelectronic devices.

## Acknowledgements

This research was financially supported by the EU Graphene Flagship (Graphene Core 3, 881603), ERC Consolidator Grant (T2DCP, 819698), H2020-EU.1.2.2.– FET Proactive Grant (LIGHT-CAP, 101017821), the European Union's Horizon 2020 research and Innovation programme (EMERGE, 101008701), the Center for Advancing Electronics Dresden (cfaed) and the DFG-SNSF Joint Switzerland-German Research Project (EnhanTopo, No. 429265950).

Open Access funding enabled and organized by Projekt DEAL.

## Conflict of Interest

The authors declare no conflict of interest.

## Keywords

boron doping, bottom-up synthesis, electronic structures, graphene nanoribbon, polycyclic aromatic hydrocarbons

Received: July 7, 2022
Revised: August 4, 2022
Published online:

[1] L. Chen, Y. Hernandez, X. Feng, K. Müllen, *Angew. Chem., Int. Ed.* **2012**, *51*, 7640.
[2] A. K. Geim, K. S. Novoselov, *Nat. Mater.* **2007**, *6*, 183.
[3] K. S. Novoselov, V. I. Fal'Ko, L. Colombo, P. R. Gellert, M. G. Schwab, K. Kim, *Nature* **2012**, *490*, 192.
[4] X.-Y. Wang, A. Narita, K. Müllen, *Nat. Rev. Chem.* **2017**, *2*, 0100.
[5] Y. Dai, Y. Liu, K. Ding, J. Yang, *Mol. Phys.* **2018**, *116*, 987.
[6] H. Luo, G. Yu, *Chem. Mater.* **2022**, *34*, 3588.
[7] Y. Gu, Z. Qiu, K. Müllen, *J. Am. Chem. Soc.* **2022**, *144*, 11499.
[8] M. Shekhirev, A. Sinitskii, *Phys. Sci. Rev.* **2017**, *2*, 20160108.
[9] Z. Chen, A. Narita, K. Müllen, *Adv. Mater.* **2020**, *32*, 2001893.
[10] A. Narita, X. Feng, K. Müllen, *Chem. Rec.* **2015**, *15*, 295.
[11] I. Ivanov, Y. Hu, S. Osella, U. Beser, H. I. Wang, D. Beljonne, A. Narita, K. Müllen, D. Turchinovich, M. Bonn, *J. Am. Chem. Soc.* **2017**, *139*, 7982.
[12] K. Nakada, M. Fujita, G. Dresselhaus, M. S. Dresselhaus, *Phys. Rev. B* **1996**, *54*, 17954.
[13] V. Barone, O. Hod, G. E. Scuseria, *Nano Lett.* **2006**, *6*, 2748.
[14] Y.-W. Son, M. L. Cohen, S. G. Louie, *Nature* **2006**, *444*, 347.
[15] J. Liu, X. Feng, *Angew. Chem., Int. Ed.* **2020**, *59*, 23386.
[16] A. Keerthi, C. Sánchez-Sánchez, O. Deniz, P. Ruffieux, D. Schollmeyer, X. Feng, A. Narita, R. Fasel, K. Müllen, *Chem. - Asian J.* **2020**, *15*, 3807.
[17] X.-Y. Wang, X. Yao, A. Narita, K. Müllen, *Acc. Chem. Res.* **2019**, *52*, 2491.
[18] M. Hirai, N. Tanaka, M. Sakai, S. Yamaguchi, *Chem. Rev.* **2019**, *119*, 8291.
[19] J. Guo, Y. Yang, C. Dou, Y. Wang, *J. Am. Chem. Soc.* **2021**, *143*, 18272.
[20] M. Ito, S. Shirai, Y. Xie, T. Kushida, N. Ando, H. Soutome, K. J. Fujimoto, T. Yanai, K. Tabata, Y. Miyata, H. Kita, S. Yamaguchi, *Angew. Chem., Int. Ed.* **2022**, *61*, e202201965.
[21] E. Von Grotthuss, A. John, T. Kaese, M. Wagner, *Asian J. Org. Chem.* **2018**, *7*, 37.
[22] K. Matsuo, S. Saito, S. Yamaguchi, *J. Am. Chem. Soc.* **2014**, *136*, 12580.
[23] J. M. Farrell, C. Mützel, D. Bialas, M. Rudolf, K. Menekse, A.-M. Krause, M. Stolte, F. Würthner, *J. Am. Chem. Soc.* **2019**, *141*, 9096.
[24] J.-J. Zhang, M.-C. Tang, Y. Fu, K.-H. Low, J. Ma, L. Yang, J. J. Weigand, J. Liu, V. W.-W. Yam, X. Feng, *Angew. Chem., Int. Ed.* **2021**, *60*, 2833.
[25] Y. Xia, M. Zhang, S. Ren, J. Song, J. Ye, M. G. Humphrey, C. Zheng, K. Wang, X. Zhang, *Org. Lett.* **2020**, *22*, 7942.
[26] Z. Huang, S. Wang, R. D. Dewhurst, N. V. Ignat'ev, M. Finze, H. Braunschweig, *Angew. Chem., Int. Ed.* **2020**, *59*, 8800.
[27] K. Yuan, R. J. Kahan, C. Si, A. Williams, S. Kirschner, M. Uzelac, E. Zysman-Colman, M. J. Ingleson, *Chem. Sci.* **2020**, *11*, 3258.
[28] R. J. Kahan, D. L. Crossley, J. Cid, J. E. Radcliffe, M. J. Ingleson, *Angew. Chem., Int. Ed.* **2018**, *57*, 8084.
[29] K. Hirano, K. Morimoto, S. Fujioka, K. Miyamoto, A. Muranaka, M. Uchiyama, *Angew. Chem., Int. Ed.* **2020**, *59*, 21448.
[30] V. M. Hertz, M. Bolte, H.-W. Lerner, M. Wagner, *Angew. Chem., Int. Ed.* **2015**, *54*, 8800.
[31] M. Ito, M. Sakai, N. Ando, S. Yamaguchi, *Angew. Chem., Int. Ed.* **2021**, *60*, 21853.
[32] D. L. Crossley, R. J. Kahan, S. Endres, A. J. Warner, R. A. Smith, J. Cid, J. J. Dunsford, J. E. Jones, I. Vitorica-Yrezabal, M. J. Ingleson, *Chem. Sci.* **2017**, *8*, 7969.
[33] K. Schickedanz, J. Radtke, M. Bolte, H.-W. Lerner, M. Wagner, *J. Am. Chem. Soc.* **2017**, *139*, 2842.
[34] C. Dou, S. Saito, K. Matsuo, I. Hisaki, S. Yamaguchi, *Angew. Chem., Int. Ed.* **2012**, *51*, 12206.
[35] K. Fujimoto, J. Oh, H. Yorimitsu, D. Kim, A. Osuka, *Angew. Chem., Int. Ed.* **2016**, *55*, 3196.
[36] H. Hirai, K. Nakajima, S. Nakatsuka, K. Shiren, J. Ni, S. Nomura, T. Ikuta, T. Hatakeyama, *Angew. Chem., Int. Ed.* **2015**, *54*, 13581.
[37] F. Miyamoto, S. Nakatsuka, K. Yamada, K.-I. Nakayama, T. Hatakeyama, *Org. Lett.* **2015**, *17*, 6158.
[38] J. Radtke, K. Schickedanz, M. Bamberg, L. Menduti, D. Schollmeyer, M. Bolte, H.-W. Lerner, M. Wagner, *Chem. Sci.* **2019**, *10*, 9017.
[39] J.-J. Zhang, L. Yang, F. Liu, Y. Fu, J. Liu, A. A. Popov, J. Ma, X. Feng, *Angew. Chem., Int. Ed.* **2021**, *60*, 25695.
[40] S. Kawai, S. Saito, S. Osumi, S. Yamaguchi, A. S. Foster, P. Spijker, E. Meyer, *Nat. Commun.* **2015**, *6*, 8098.
[41] R. R. Cloke, T. Marangoni, G. D. Nguyen, T. Joshi, D. J. Rizzo, C. Bronner, T. Cao, S. G. Louie, M. F. Crommie, F. R. Fischer, *J. Am. Chem. Soc.* **2015**, *137*, 8872.
[42] E. Carbonell-Sanromà, A. Garcia-Lekue, M. Corso, G. Vasseur, P. Brandimarte, J. Lobo-Checa, D. G. De Oteyza, J. Li, S. Kawai, S. Saito, S. Yamaguchi, J. E. Ortega, D. Sánchez-Portal, J. I. Pascual, J. I. Pascual, *J. Phys. Chem. C* **2018**, *122*, 16092.
[43] E. Carbonell-Sanroma, P. Brandimarte, R. Balog, M. Corso, S. Kawai, A. Garcia-Lekue, S. Saito, S. Yamaguchi, E. Meyer, D. Sanchez-Portal, J. I. Pascual, *Nano Lett.* **2017**, *17*, 50.
[44] N. Friedrich, P. Brandimarte, J. Li, S. Saito, S. Yamaguchi, I. Pozo, D. Peña, T. Frederiksen, A. Garcia-Lekue, D. Sánchez-Portal, J. I. Pascual, J. I. Pascual, *Phys. Rev. Lett.* **2020**, *125*, 146801.
[45] P. Zhang, X. Li, J. Dong, M. Zhu, F. Zheng, J. Zhang, *Appl. Phys. Lett.* **2022**, *120*, 132406.
[46] S. Kawai, S. Nakatsuka, T. Hatakeyama, R. Pawlak, T. Meier, J. Tracey, E. Meyer, A. S. Foster, *Sci. Adv.* **2018**, *4*, eaar7181.
[47] X.-Y. Wang, J. I. Urgel, G. B. Barin, K. Eimre, M. Di Giovannantonio, A. Milani, M. Tommasini, C. A. Pignedoli, P. Ruffieux, X. Feng, R. Fasel, K. Müllen, A. Narita, *J. Am. Chem. Soc.* **2018**, *140*, 9104.
[48] L. Jin, N. Bilbao, Y. Lv, X.-Y. Wang, P. Soltani, K. S. Mali, A. Narita, S. De Feyter, K. Müllen, Z. Chen, *Chem. Commun.* **2021**, *57*, 6031.
[49] Y. Fu, H. Yang, Y. Gao, L. Huang, R. Berger, J. Liu, H. Lu, Z. Cheng, S. Du, H.-J. Gao, X. Feng, *Angew. Chem., Int. Ed.* **2020**, *59*, 8873.
[50] G. Li, K.-Y. Yoon, X. Zhong, J. Wang, R. Zhang, J. R. Guest, J. Wen, X.-Y. Zhu, G. Dong, *Nat. Commun.* **2018**, *9*, 1687.
[51] R. D. Mccurdy, P. H. Jacobse, I. Piskun, G. C. Veber, D. J. Rizzo, R. Zuzak, Z. Mutlu, J. Bokor, M. F. Crommie, F. R. Fischer, *J. Am. Chem. Soc.* **2021**, *143*, 4174.

 

Jin-Jiang Zhang, after obtaining his Master's degree in Organic Chemistry from Xi'an Jiaotong University in 2018, joined the group of Xinliang Feng at Technische Universität Dresden as a Ph.D. student. His research interests are the development novel methodologies to precisely synthesize boron-doped polycyclic aromatic hydrocarbons, boron-doped graphene nanoribbons as well as their applications in organic nanoelectronics.

Ji Ma received his Ph.D. degree in Synthetic Chemistry under the supervision of Xinliang Feng from Technische Universität Dresden in 2019. In the same year, he was appointed as a research group leader at the Chair of Molecular Functional Materials at the Technische Universität Dresden. His research interests are the precision synthesis of novel polycyclic hydrocarbons, nanographenes, graphene nanoribbons, and heteroatom-doped carbon nanostructures as well as their applications in organic nanoelectronics and the emerging organic spintronic fields.

Xinliang Feng has been Full Professor and the Head of the Chair of Molecular Functional Materials at Technische Universität Dresden since 2014. Starting from 2021, he has been the Director of Max Planck Institute of Microstructure Physics (Halle), Germany. His current scientific interests include organic synthesis, supramolecular chemistry of $\pi$-conjugated systems, bottom-up synthesis and top-down fabrication of graphene and graphene nanoribbons, 2D polymers and supramolecular polymers as well as 2D carbon-rich conjugated polymers for (opto)electronic applications and materials for energy storage and conversion.